THE CRYSTAL CHEMISTRY OF DEFECT-STRUCTURED METEORITIC HIBONITE: ATOMIC RESOLUTION IMAGING AND X-RAY MAPPING. L. P. Keller[1], A. Yasuhara[2], J. Han[3], and E. L. Keller[4]. [1]ARES, Code XI3, NASA-JSC, 2101 NASA Parkway, Houston, TX 77058, USA (Lindsay.P.Keller@nasa.gov), [2]JEOL, 3-1-2 Musashino, Akishima, Tokyo, 196-8558, Japan, [3]USRA Lunar and Planetary Institute, 3600 Bay Area Boulevard, Houston, TX 77058, USA, [4]Dept. Chemistry, U. Minn., Minneapolis, MN 55455, USA.

Introduction: Hibonite ($CaAl_{12}O_{19}$) is a primary refractory phase occurring in many Ca-Al-rich inclusions (CAIs) and is a predicted early condensate in the cooling solar nebula. Our previous microstructural studies of hibonite in CAIs and their Wark-Lovering rims revealed a distinctive microstructure consisting of numerous extended defects along (001) that are interpreted as complex intergrowths of stoichiometric and non-stoichiometric (Ca-deficient, Al-rich) hibonites [1-4]. Defect-structured hibonite is metastable, but apparently more kinetically-favored than the thermodynamically predicted equilibrium phase assemblages of hibonite+corundum or hibonite+spinel. Han et al. [3] showed that minor Mg stabilized the defect-structured hibonite and that the formation of these extended defects is controlled by rapid cooling from high temperature thermal processes, but many questions remain. In this study, we obtained atomic-scale imaging and chemical data using next-generation analytical electron microscopy to determine the structure and bonding in the defects and the role of Mg and Ti in their formation.

Samples and Methods: We analyzed a focused ion beam (FIB) section extracted from part of a large compact Type A CAI from Allende. Hibonite occurs in the base layer of the Wark-Lovering rim, but also as lath-shaped grains intergrown with spinel and perovskite as inclusions in coarse-grained melilite. We studied a zoned hibonite grain from the CAI interior. The FIB section was analyzed using a JEOL 2500SE scanning, transmission electron microscope (STEM) at JSC, and a JEOL F200 STEM at JEOL in Japan. The F200 is equipped with a cold FEG source, high angle annular darkfield (HAADF) detector, dual 100 mm^2 silicon drift detectors, and a Gatan imaging filter for electron energy loss spectroscopy (EELS). We obtained atomic resolution HAADF images, energy dispersive X-ray maps, and EELS data from an Allende CAI hibonite grain and from an experimental sample of defect-structured hibonite [3]. Following the high-resolution imaging of the microstructures, we then mapped regions of interest that contained defects using a 150 pA, 0.1 nm probe, with a 0.02 s dwell time/pixel. Successive image frames were added until acceptable counting statistics were achieved (typically <5 min).

Results and Discussion: X-ray mapping with a scanning electron microscope (SEM) revealed μm-scale oscillatory zoning in the Allende hibonite grain, with MgO and TiO_2 contents up to 3.2 wt.% and 7.2 wt.%, repectively. FIB/TEM analysis of this hibonite grain exhibits a complex microstructure with numerous defects along the c-axis that show a 1.6 nm lattice spacing and contribute to strong streaking along c* in electron diffraction patterns, similar to our previous high-resolution TEM work [3,4]. The defects are concentrated in regions with higher Mg and Ti contents.

The hibonite structure contains 5 different Al sites: three octahedral sites (M1, M4, and M5), a trigonal bipyramidal site (M2), and a tetragonal site (M3). The hibonite structure consists of alternating Ca blocks with a composition of $CaAlO_3^-$ and "spinel" blocks with a composition of $Al_{11}O_{16}^+$. The Ca block contains the M2 and M4 Al sites, and the spinel block contains four close packed O layers with the M1, M3, and M5 Al sites in interstices. Schmid and De Jonghe [5] proposed a model for the defect structure with a wider spinel block containing six close packed O layers, but the occupancy and coordination of the additional Al sites in their model was not described.

The HAADF images can be interpreted in terms of the distribution of heavy elments ($z > 8$) in the hibonite structure. We used CrystalMaker™ software to plot heavy atom positions in the same crystallographic orientation as the HAADF images using single crystal structure data from [6]. There is excellent correspondence between the atomic resolution HAADF images and the heavy atom locations in the hibonite structure, and so we interpret the structure of the defect as an additional M5 layer and [M1+M3] layer (Fig. 1). In our model, the wider spinel block in the defect contains twice as many M1 and M3 sites, and 50% more M5 sites as the spinel block in stoichiometric hibonite.

From single crystal X-ray diffraction studies of hibonite, it is inferred that Mg occurs predominantly on the tetrahedral M3 site and the Ti prefers the distorted tetragonal bypyramid M2 site [e.g. 7]. We have directly mapped the atomic distribution of Mg and Ti in stoichiometric and defect-structured hibonite (Fig. 2) and show that Mg is largely concentrated in the tetragonal M3 sites, but also in the neighboring M5 octahedral sites. Likewise, X-ray mapping shows that Ti is concentrated in the M2 sites in the same crystallographic plane as the Ca atoms although the linescans suggest some Ti must occupy the M4 sites as well. The additional M3 sites result in a defect structure that can

accommodate higher Mg levels.

EELS data from the Ti $L_{2,3}$ edge in the hibonite and the adjoining perovskite were obtained using a JEOL F200 with an energy resolution of 0.4eV FWHM at the zero loss peak. The perovskite spectrum is consistent with Ti^{4+}, but the hibonite spectrum shows distinct low energy shoulders on the two L_3 peaks that we interpret as a contribution of Ti^{3+} (Fig. 3). We quantified the Ti^{3+}/Ti^{4+} ratio by peak-fitting of the spectrum and we estimate that ~15-20% of the Ti is present as Ti^{3+}. Ti is not associated with the defects and likely has only a minor role in their formation as part of the charge-coupled substitution MgTi for AlAl.

Conclusions: Our previous work indicates that Mg, and possibly Ti, play a role in stabilizing defect-structured hibonite, but the structure and bonding in the defects was largely unknown. Using our new observations, we propose a defect model with twice as many M1 and M3 sites, and 50% more M5 sites compared to the spinel block in stoichiometric hibonite. The defect structure is the critical crystallographic feature allowing greater Mg incorporation and accounts for the common occurrence of defect-structured hibonite in CAIs.

Acknowledgements: This study was supported by NASA grants EW14-2-122 to LPK. We thank JEOL for access to the F200 STEM.

References: [1] Keller L. P. (1991) *AGU* 72, 141. [2] Han J. et al. (2015) *MAPS* 50, 2121. [3] Han J. et al. (2016) *LPSC* 47, #2848. [4] Han J. et al. (2016) *79th MetSoc* #6534. [5] Schmid H. & De Jonghe L. C. (1983) *Phil. Mag. A* 48, 287. [6] Nagashima, M. et al. (2010) *Min. Mag*. 74, 871. [7] Giannini, M. et al. (2014) *Am. Min*. 99, 2060.

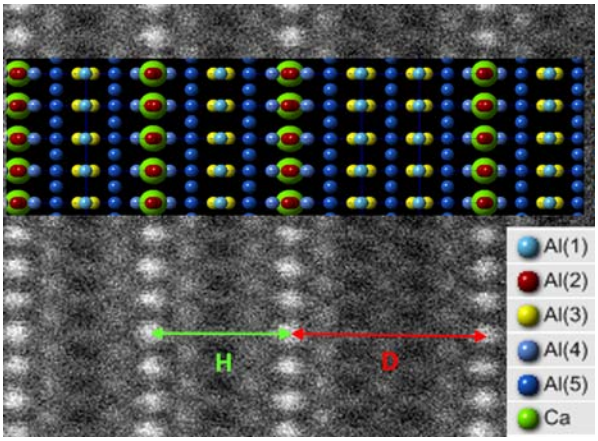

Figure 1. HAADF image from the [110] of hibonite showing stoichiometric hibonite (H) and an extended defect (D). The inset shows the distribution of heavy elements in hibonite and our model for the atomic arrangement in the defect.

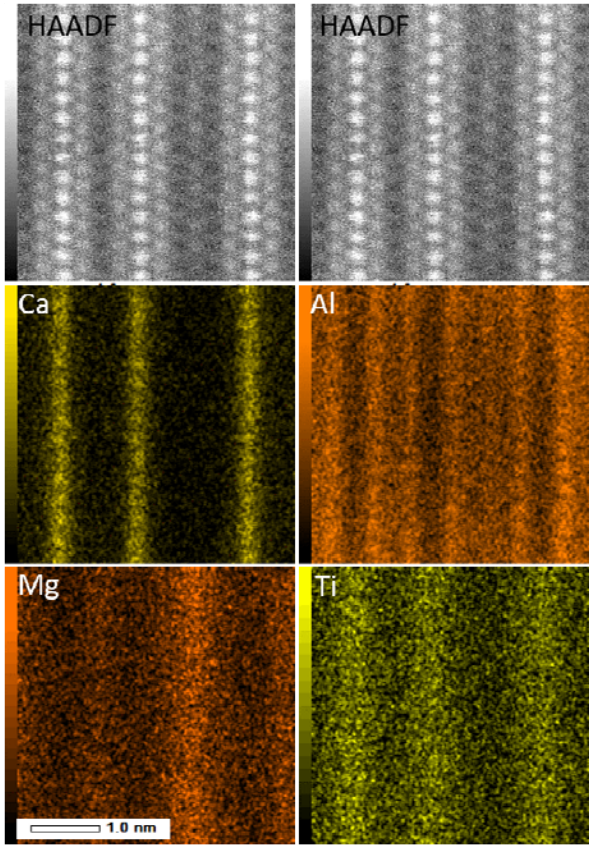

Figure 2. HAADF images and corresponding X-ray maps for Ca, Al, Mg, and Ti in meteoritic hibonite. Mg is concentrated in the defects but Ti occurs within the Ca block.

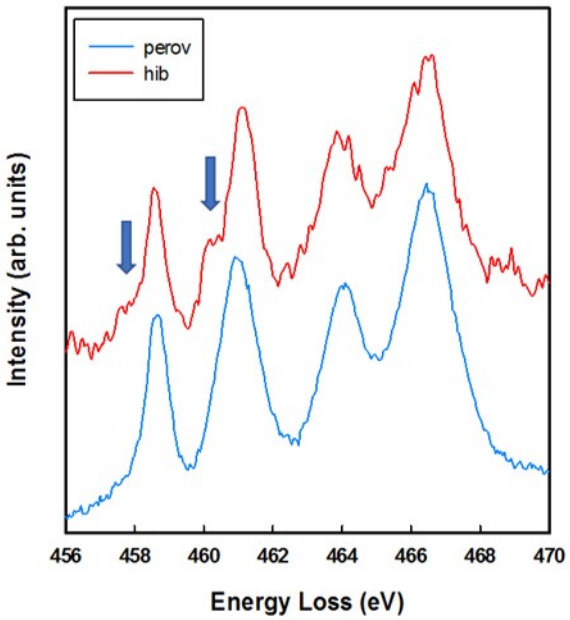

Figure 3. EELS spectra from the Ti $L_{2,3}$ edge in meteoritic perovskite (blue) and hibonite (red). The low energy shoulders indicated by blue arrows are consistent with the presence of Ti^{3+} in hibonite.